Research article

Carbon Future

Cu nanoparticles embedded in fluorinated mesoporous carbon for enhanced CO_2 electroreduction to C_2 products

Yao Ma[#], Taishi Xiao[#], Kerun Zhu, Dongyuan Zhao, and Wei Li

Department of Chemistry, Laboratory of Advanced Materials, Shanghai Key Laboratory of Molecular Catalysis and Innovative Materials, State Key Laboratory of Molecular Engineering of Polymers, and iChEM, Fudan University, Shanghai 200433, China

Cite This: *Carbon Future* **2025**, *2*, 9200034

Read Online

ABSTRACT: The utilization of renewable electricity to drive the electrochemical CO_2 reduction reaction (CO_2RR) presents an attractive avenue for achieving carbon neutrality, as it facilitates the conversion of CO_2 into valuable chemicals and fuels. However, producing high-energy-density multi-carbon hydrocarbon products (C_{2+}) still suffers from low selectivity, and the process proves highly sensitive to both catalyst structure and electrolyte conditions. Here, we report the synthesis of fluorinated mesoporous carbon-confined copper nanoparticles (Cu@F-MC) via a bottom-up molecular self-assembly and carbonization strategy. The Cu@F-MC catalyst established a two-dimensional (2D) mesoporous structure with well-dispersed 6.5 nm-wide mesopores and a high surface area. The confinement effect of mesoporous carbon enabled the small size and well dispersion of Cu nanoparticles (~ 10 nm). The fluorine-doped structure not only effectively inhibited the side hydrogen evolution reaction, but also modulated the local electronic structures of Cu nanoparticles toward multi-carbon product generation. Thus, the Cu@F-MC exhibited a high current density of 500 mA·cm^{-2} with an ethanol Faradaic efficiency (FE) of 40% for CO_2 reduction in a flow cell, and a prolonged stability with over 50% selectivity for $FE_{C_{2+}}$ during a 70h continuous electrolysis in the membrane electrode assembly test. This strategy offers a promising approach to concurrently improve the selectivity and stability of copper-based catalysts in CO_2RR.

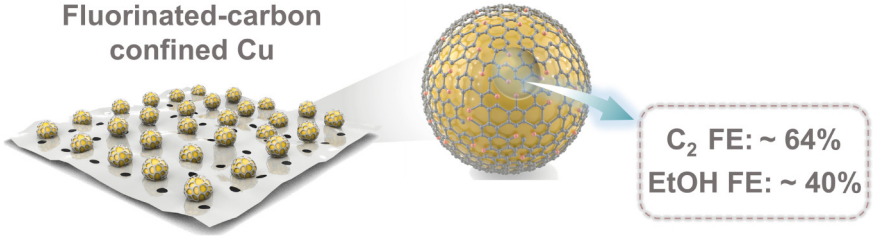

KEYWORDS: copper catalyst, fluorine, mesoporous carbon, confinement, CO_2RR

1 Introduction

The conversion of CO_2 into fuels and chemicals holds significant promise for alleviating the depletion of fossil resources and reducing carbon emissions[1–3]. The synthesis of multi-carbon (C_{2+}) products such as ethylene and ethanol from CO_2 is particularly appealing due to their versatility in the chemical and energy industries[4–7]. While catalytic hydrogenation of CO_2 with H_2 at high temperatures and pressures can yield C_{2+} products, this thermo-catalytic process faces challenges including broad distributions of C_{2+} products, as well as the undesired formation of CH_4 and CO. To overcome these limitations, the electrocatalytic CO_2 reduction reaction (CO_2RR) with water using renewable electricity emerges as a promising route for CO_2 utilization under ambient conditions[8, 9]. Electrochemical processes offer potential advantages, potentially providing better control over C_{2+} product distribution compared to thermo-catalytic reactions[10–12]. However, despite recent advancements in electrocatalytic CO_2RR lead to C_{2+} products, challenges persist with limited C_{2+} selectivity as well as short catalyst lifespan. The stable C_{2+} yield in electrocatalytic CO_2RR generally remains lower than that of reported thermo-catalytic processes.

Copper stands out as the most selective catalyst for the electrocatalytic CO_2 reduction to yield C_{2+} products[13–15]. Numerous strategies, including morphology and facet engineering, vacancy steering, dopant modification, bimetallic catalysis, and electrolyte design, have been devised to enhance the efficiency of copper catalysts in facilitating C_{2+} formation[16–19]. Despite reported high Faradaic efficiencies (FEs) for C_{2+} products, the overall activity remains modest, and the operational range is typically narrow. Some studies have achieved elevated current densities (> 100 mA·cm^{-2}) in the CO_2RR to C_{2+} products by utilizing a flow cell with a gas diffusion electrode (GDE) to overcome the CO_2 solubility limit in aqueous solutions[20–23]. However, the development of more efficient electrocatalysts that align with commercial requirements remains a pivotal challenge. The primary issue with promising Cu-based electrocatalysts is their tendency for uncontrollable reconstruction, which causes the ambiguous active sites and an ephemeral lifetime[24, 25].

Received: November 7, 2024; **Revised:** December 26, 2024
Accepted: January 6, 2025

Address correspondence to Wei Li, weilichem@fudan.edu.cn
[#]Yao Ma and Taishi Xiao contributed equally to this work.

https://doi.org/10.26599/CF.2025.9200034

Inspired by the "chain mail" design, various strategies have been employed to stabilize Cu catalysts and prevent the reconstruction of predesigned active sites, such as carbon confinement[26–28]. However, these strategies are still limited by the trade-off between high stability and high activity of Cu catalysts, as the carbon shield inevitably leads to the metal sites being partially screened[29, 30]. Hence, designing a carbon shield that overcomes activity limitations while maintaining highly exposed metal sites and enhanced stability plays a crucial role in promoting the performance of Cu-based catalysts in CO_2 electroreduction.

Here, we synthesized a fluorinated two-dimensional (2D) mesoporous carbon-confined copper nanoparticle catalyst. The small-sized (~ 10 nm) and well-dispersed Cu nanoparticles were achieved through the confinement effect of mesoporous carbon. The fluorine-modified carbon framework effectively surpassed the competing hydrogen evolution reaction (HER), and created a modulated local electronic field around the Cu nanoparticles, resulting in the preferred catalytic property for C_{2+} products. As a result, the fluorinated mesoporous carbon-confined Cu nanoparticles (Cu@F-MC) demonstrated an impressive ethanol Faradaic efficiency of 40% at a current density of 500 mA·cm^{-2} in a flow cell, along with a prolonged stability with over 50% C_{2+} product formation even under high current conditions during 70h continuous electrolysis. Additionally, the selectivity and stability toward C_2 products were further enhanced by the cation modifications via negative interface provided by fluorine-rich carbon interface. This strategy highlights the potential of the multifunctional mesoporous carbon-cooperated Cu catalyst to pave a new way for boosted C_2 products generation.

2 Results and discussion

The Cu@F-MC was prepared through a molecular self-assembly method by using F-resol as the carbon precursor (**Fig. 1**)[31]. In the preparation process, F-resol was used as the carbon source and Pluronic F127 as the mesoporous structure template. Copper nitrate was dissolved in tetrahydrofuran (THF) solution, and tannic acid was added to serve as a ligand to anchor the Cu ions and form Cu–O coordination bonds. During calcination, the relatively stable Cu–O coordination interactions maintain the small-sized copper particles even at 700 °C. The resulting solution was then assembled at the interface of sodium chloride. Finally, the mixture underwent high-temperature carbonization to obtain the Cu@F-MC product. Transmission electron microscopy (TEM) image illustrates that the Cu nanoparticles are confined and evenly dispersed in the mesoporous carbon matrix with a particle size of 7–9 nm (**Figs. 2**a and 2b). The X-ray diffraction (XRD) patterns of Cu@F-MC exhibit diffraction peaks that correspond well to the cubic phase of Cu (PDF #00-004-0836) and the cubic phase of Cu_2O (PDF #01-078-2076), without other impurities (Fig. 2h). Due to the poor stability of Cu under air conditions which leads to its oxidation, the appearance of Cu_2O phase is observed. Furthermore, high-resolution TEM (HRTEM) images of Cu@F-MC show clear lattice fringes with the spacings of 0.21, 0.24, and 0.36 nm, corresponding to the (111) plane of Cu and (200) plane of graphite carbon, respectively (Fig. 2c). High-angle annular dark-field scanning transmission electron microscopy (HAADF-STEM, Figs. 2d–2g) and corresponding energy-dispersive X-ray spectroscopy (EDS) mappings verify that the Cu, F, and C elements are homogeneously distributed along the mesoporous carbon matrix.

In the Fourier-transform infrared (FT-IR) spectrum of Cu@F-MC, distinctive peaks are evident at 635, 1634, and 3425 cm^{-1}, corresponding to the vibrations of C–H bonds, C–C bonds, and OH, respectively. Particularly, a pronounced peak exists at approximately 1050 cm^{-1}, associated with the characteristic vibration of C–F bond, verifying the truly introduction of fluorine in mesoporous carbon framework (**Fig. 3**a)[32]. N_2 adsorption–desorption isotherms of Cu@F-MC exhibit a characteristic type IV curve, indicative of the mesoporous structure. Calculations reveal that the Cu@F-MC possesses a Brunauer–Emmett–Teller (BET) surface area of 612 m^2·g^{-1} and a pore volume of 0.47 cm^3·g^{-1} (Fig. 3b). The pore size distribution curve indicates an average pore size of ~ 6.5 nm for the Cu@F-MC (inset in Fig. 3b). To elucidate the chemical environment of the Cu@F-MC, X-ray photoelectron spectroscopy (XPS) characterization was conducted. The survey spectra reveal prominent peaks corresponding to Cu, C, F, and O elements (Fig. 3c). The surface fluorine content measured by XPS for the Cu@F-MC catalyst is approximately 1.0 wt.%. In the high-resolution Cu 2p spectrum, three doublets around 932.5, 935.1, and

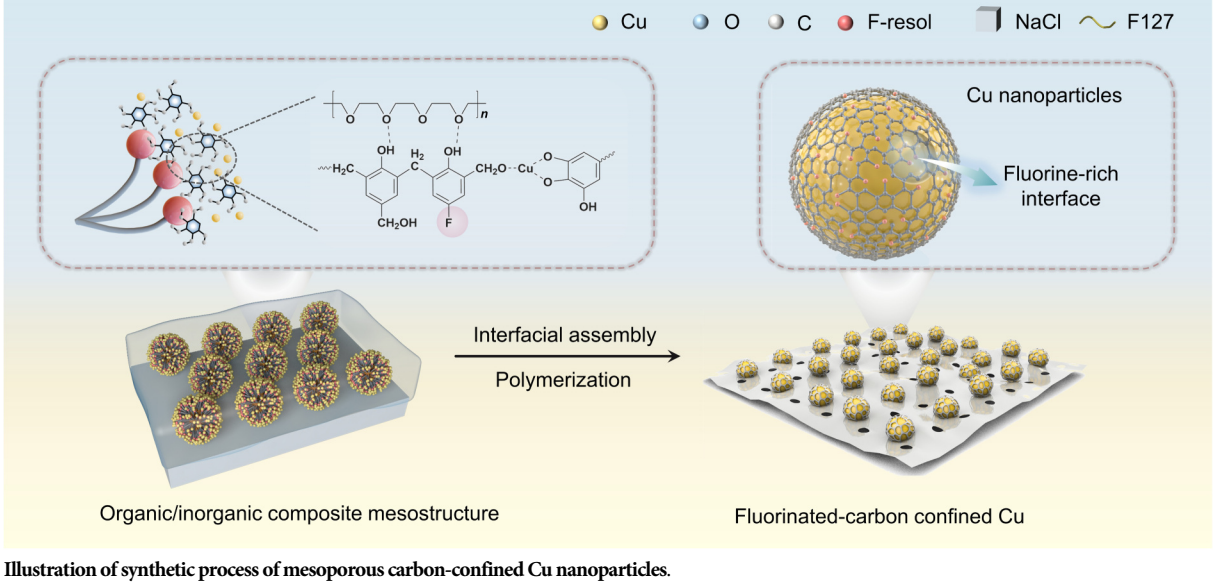

Fig. 1. Illustration of synthetic process of mesoporous carbon-confined Cu nanoparticles.

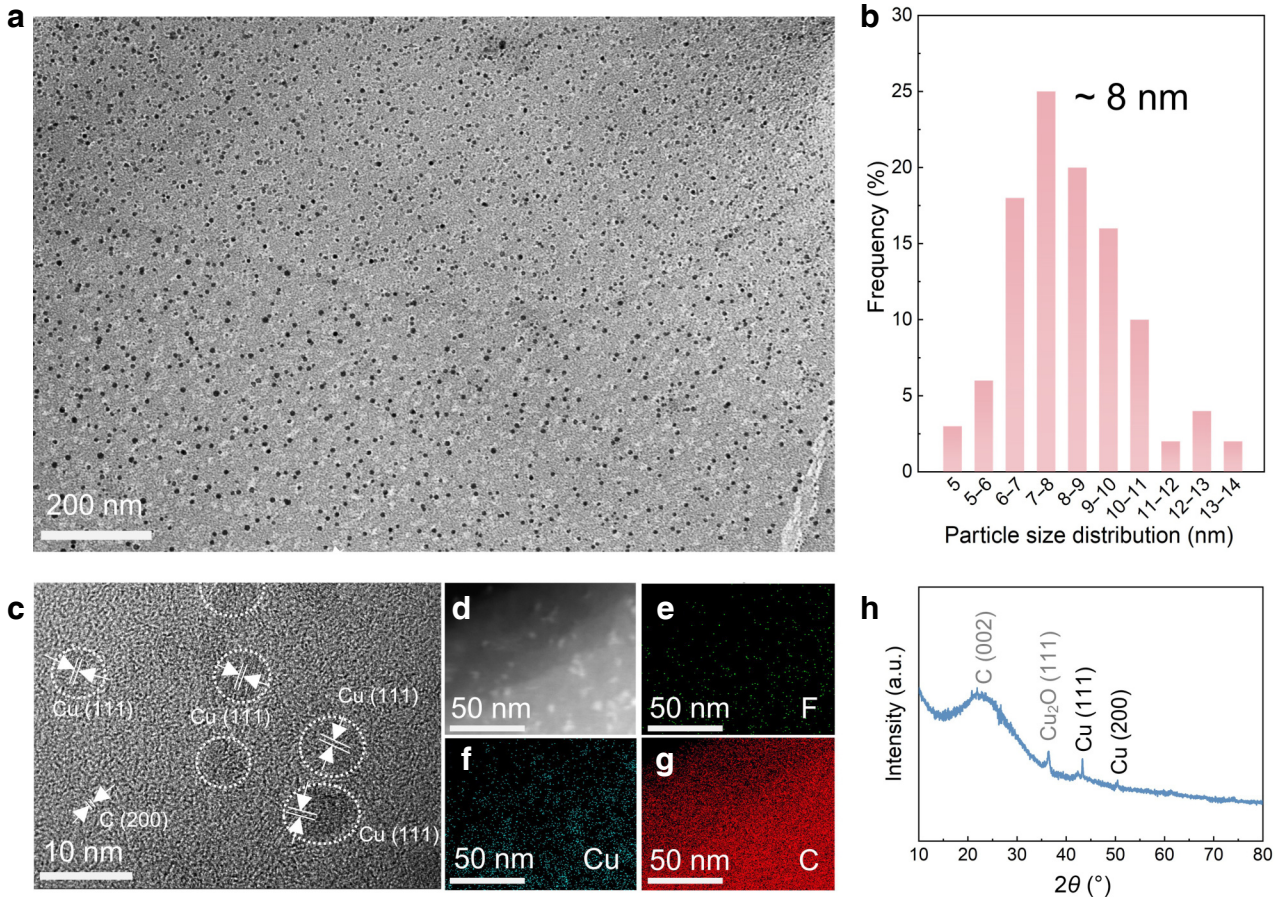

Fig. 2. Characterizations of Cu@F-MC. a–g, TEM image (a), statistics of particle size distribution of Cu nanoparticles (b), HRTEM image (c), and EDS elemental mapping images ((d)–(g)) of Cu@F-MC. **h,** XRD patterns of Cu@F-MC.

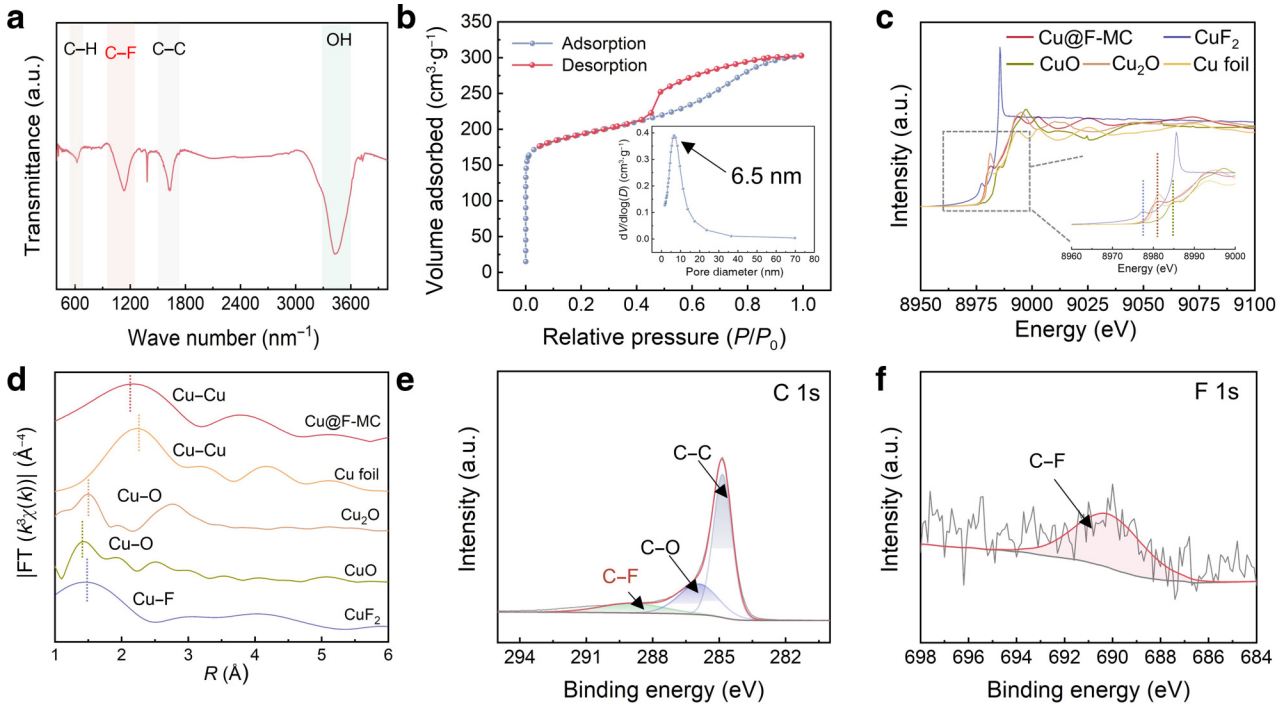

Fig. 3. Porous structure and coordination environment of Cu@F-MC. a, FT-IR spectrum of Cu@F-MC. **b**, Nitrogen adsorption–desorption isotherms of Cu@F-MC. The inset is the corresponding pore size distribution. **c**, Cu K-edge XANES spectra. **d**, Fourier-transform EXAFS spectra of Cu@F-MC, CuF_2, Cu_2O, CuO, and Cu foil. **e**, **f**, XPS spectra of C 1s (e) and F 1s (f) for Cu@F-MC.

938.2 eV are assignable to Cu(0), Cu(I), and Cu(II), respectively (Fig. 3d). Notably, the C 1s spectrum (Fig. 3e) displays three deconvoluted peaks representing C–O, C–C, and C–F bonds. In the F 1s spectrum, a distinct peak corresponding to the C–F bond is also observed (Fig. 3f)[33, 34]. The existence of C–F bond confirms the strong interaction between fluorine and carbon support, consistent with the previous results. The X-ray absorption near-edge structure (XANES) of Cu K-edge in Cu@F-MC catalysts exhibits a resemblance to Cu_2O, which indicates the Cu(I) dominated chemical state. Typically, the characteristic peak in pre-edge (~ 8981 eV) is stronger than that in Cu_2O (Supplementary Fig. S1a). Furthermore, extended X-ray adsorption fine structure (EXAFS) spectra in *R* space of Cu display a prominent peak around 2.1 Å in Cu@F-MC, assigned to the Cu–Cu bond (Supplementary Fig. S1b). The Cu–Cu bond scattering path is shorter than that in Cu foil, and this shortened length may origins from the fluorine-rich local state of Cu@F-MC catalysts. Additionally, the absence of Cu–F scattering in Cu@F-MC suggests that fluorine predominantly forms C–F bonds rather than directly coordinates with copper.

As a control, Cu@F-MC catalysts with varying Cu nanoparticle sizes can be synthesized by adjusting the content of Cu and tannin. Consequently, the size of dispersed Cu nanoparticles ranges from 8 to 100 nm, depending on the coordination interactions between tannin and Cu (Supplementary Figs. S2 and S3). This bottom-up strategy efficiently confines Cu nanoparticles within a tunable size distribution. To delineate the impact of fluorine in mesoporous carbon, we synthesized a copper catalyst confined within fluorine-free mesoporous carbon (Cu@MC) and post-loaded Cu in fluorinated mesoporous carbon (F-MC + Cu) using a comparable method. The XANES of Cu K-edge of Cu@MC and F-MC + Cu has obvious change compared to that of Cu@F-MC (Supplementary Fig. S1c). Specifically, the characteristic peak in pre-edge has notable positive shift in Cu@MC and F-MC + Cu in comparison to that in Cu@F-MC, indicating the higher chemical state of Cu. In the EXAFS in *R* space of Cu, the scattering signals in Cu@MC and F-MC + Cu are primarily dominated by Cu–O bonds, which is a clear contrast to the Cu–Cu bond signals present in Cu@F-MC (Supplementary Fig. S1c).

To analyze the catalytic preference between CO_2RR and HER, electrochemical performance in a GDE-based flow cell was tested. Gas chromatography (GC) and hydrogen nuclear magnetic resonance (^{1}H NMR) were employed for analysis of both gaseous and liquid products. The resulting FEs indicate that Cu@F-MC exhibits a strong suppression on the HER. It is evident that the FE of H_2 consistently remains below 30% among a wide potential window for different Cu loadings of the Cu@F-MC catalysts (Supplementary Fig. S4). The partial current density of C_2 (j_{C_2}) was found to be positively correlated with the loadings of small Cu nanoparticles. However, as the Cu loading increases, the formation of large Cu aggregations leads to decreased selectivity in CO_2RR, impacted by a significant enhancement of HER. The maximum HER conversion is less than 10% at a Cu loading of 40%, and this sample is designated as Cu@F-MC for further investigation.

In the performance evaluation of Cu@MC, typical characteristics of copper-based catalysts are observed, yielding a diverse spectrum of products ranging from C_1 to C_2. However, its selectivity for individual products is modest, accompanied by a notable presence of HER. Over a broad voltage range, HER selectivity maintained around 50% (**Fig. 4a**). Within the current density range of −100 to

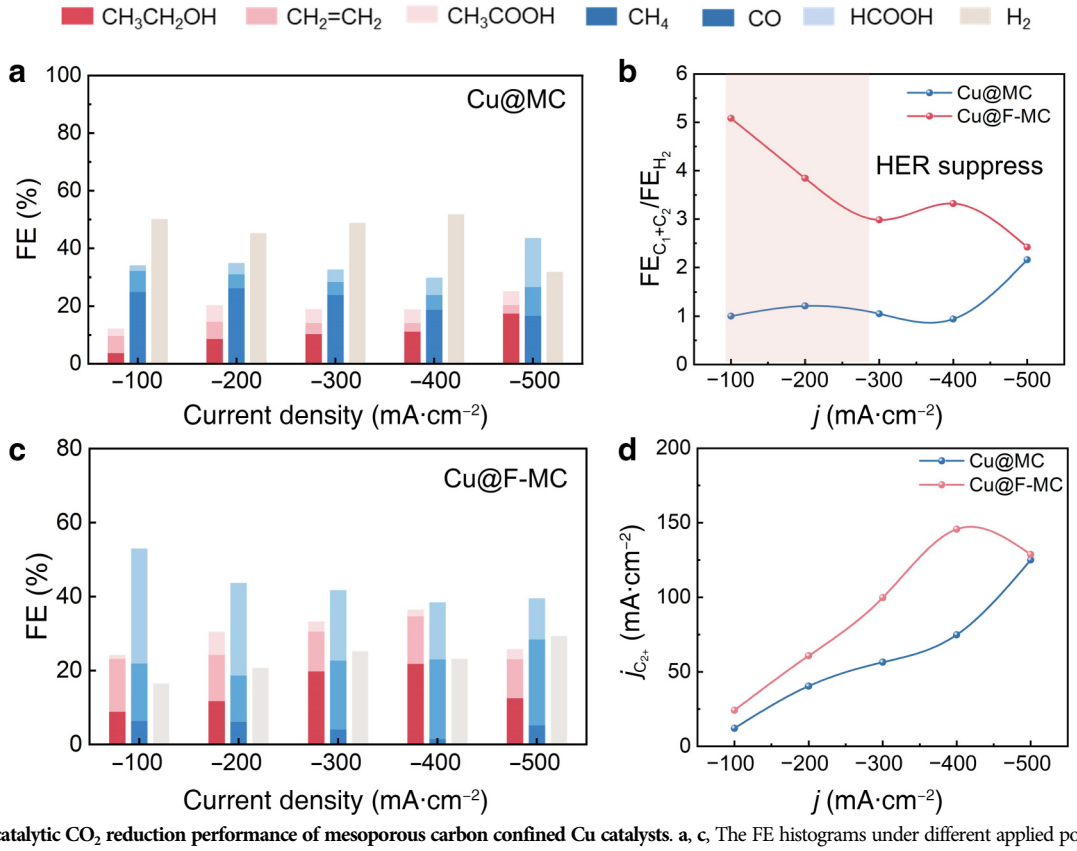

Fig. 4. Electrocatalytic CO_2 reduction performance of mesoporous carbon confined Cu catalysts. a, **c**, The FE histograms under different applied potentials in a gas-fed flow cell of Cu@MC (a) and Cu@F-MC (c). **b**, The $FE_{C_1+C_2}/FE_{H_2}$ of Cu@MC and Cu@F-MC. **d**, The partial current density of C_{2+} ($j_{C_{2+}}$) curves under different applied potentials in a gas-fed flow cell of Cu@MC and Cu@F-MC.

−500 mA·cm^{-2}, the conversion of CO_2 to hydrocarbons can exceed 80% (Fig. 4c). Specifically, at a current density of −400 mA·cm^{-2}, the selectivity of C_{2+} products reaches 40%. Upon plotting the ratio $FE_{C_1+C_2}/FE_{H_2}$ at a current density of −100 mA·cm^{-2}, it becomes evident that this value for Cu@F-MC exceeds 50%, which is four times higher than that in Cu@MC (Fig. 4b). Additionally, Fig. 4d shows that Cu@F-MC exhibits a C_{2+} partial current close to −150 mA·cm^{-2} at a total current density of −400 mA·cm^{-2}, significantly surpassing that of Cu@MC. This result strongly indicates that the introduction of fluorine effectively suppresses HER, and the fluorine-functionalized mesoporous carbon network assumes a regulatory role on copper nanoparticles, augmenting the selectivity towards C_{2+} products.

Previous studies have indicated that electron-deficient copper, due to its empty d-orbital electronic structure, facilitates the coupling of *CO to enhance the selectivity of C_{2+} products. In addition, the positive charge center of the cationic ionomer is beneficial for the activation of CO_2 and lowers the barrier for *CO coupling, promoting the generation of C_{2+} products. The local charge modulation on the catalyst surface is crucial for its selectivity and activity. However, due to the active surface reconstruction of copper nanoparticle, its surface electronic state and local charge are hard to be precisely controlled, leading to the ambiguous active sites and an ephemeral lifetime. A carbon-coated armor structure can enhance the stability of copper sites, but it inevitably limits the active centers of copper. In this regard, simultaneously regulating the skeletal properties of carbon and optimizing the surface state of copper nanoparticles is rarely reported. In the Cu@F-MC structure, the copper nanoparticles confined within fluorinated mesoporous carbon network are anticipated to retain a negatively charged interface consistent with the F-MC. This interface provides adequate sites for the adsorption and stabilization of cations molecular, and meanwhile effectively suppresses copper site reconstruction, thereby promoting the formation of C_2 products. Building upon this insight, our approach involves the modification of Cu@F-MC with imidazole-type molecules containing cationic groups to further enhance its selectivity towards C_{2+} products. The modification method is derived from previously published literature[21, 35, 36]. TEM image shows the emergence of a distinct layer of amorphous coating on the original mesoporous carbon surface, confirming the successful incorporation of cationic groups (Supplementary Fig. S5). This introduction induces a noticeable change in the surface environment of the catalyst.

The FT-IR spectra reveal that the modified Cu@F-MC/CF exhibits prominent vibration signals of C–N and N–H bonds, in addition to the peaks associated with C–F, C–C, and OH vibrations. This outcome signifies a substantial alteration in the surface microenvironment of the catalyst due to the introduction of cationic groups (**Fig. 5a**). To go insight into the electrostatic interaction between the cationic layer and Cu@F-MC, we conducted zeta potential tests. The results indicate that the original fluorine-functionalized mesoporous carbon possesses a negatively charged surface. In contrast to prior reports where the surface potential becomes positive after loading metal in Cu@F-MC, where Cu nanoparticles are confined within the mesoporous carbon, the surface retains a negative charge akin to the original fluorine-

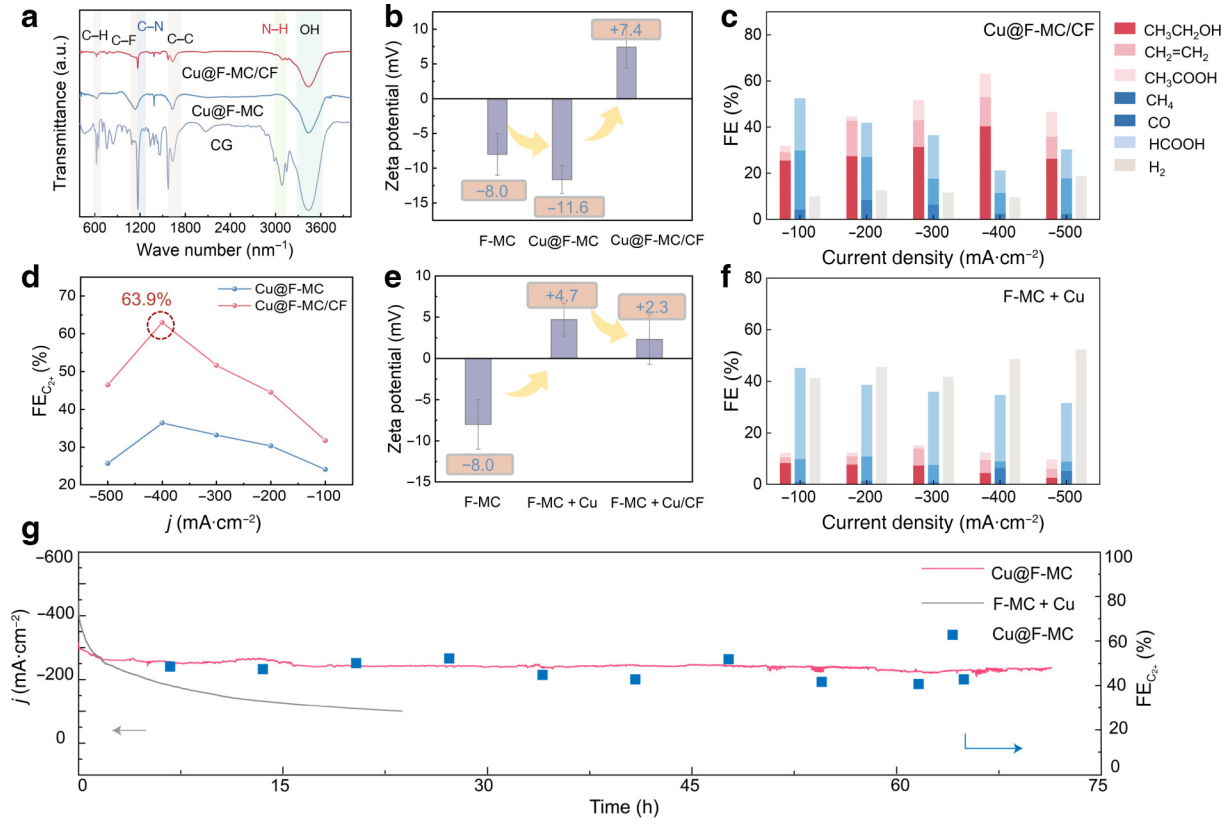

Fig. 5. Cation modification of Cu@F-MC. **a**, FT-IR spectra of CG, Cu@F-MC, and Cu@F-MC/CF. **b**, Zeta potentials of F-MC, Cu@F-MC, and Cu@F-MC/CF. **c**, **d**, The FE (c) and $FE_{C_{2+}}$ (d) of Cu@MC and Cu@F-MC/CF under different applied potentials in a gas-fed flow cell. **e**, Zeta potentials of F-MC, F-MC + Cu, and F-MC + Cu/CF. **f**, The FE of F-MC + Cu. **g**, Stability testing of Cu@F-MC and F-MC + Cu assembled MEA.

functionalized mesoporous carbon (Fig. 5b). This suggests that electrostatic interactions with cationic groups are facilitated, thus, enhancing the stability of the cationic group binding. The observed positively charged nature in the modified Cu@F-MC/CF further substantiates this conclusion.

In CO_2RR performance testing, the cation-modified Cu@F-MC/CF demonstrates a significant advantage in enhancing selectivity towards multi-carbon products compared with the unmodified Cu@F-MC. Across a broad potential range from −100 to −500 mA·cm^{-2}, hydrogen production rates consistently remain below 10%, markedly promoting the conversion of CO_2 to hydrocarbons. Notably, Cu@F-MC exhibits a dominance of C_1 product selectivity, while the cation-modified Cu@F-MC/CF presents a C_2-dominant profile. At a current density of −400 mA·cm^{-2}, the $FE_{C_{2+}}$ reaches 63.9%, surpassing the 40% observed in Cu@F-MC (Fig. 5d). Notably, $FE_{ethanol}$ consistently exceeded 20% at −100 to −500 mA·cm^{-2}, peaking at 41% at current density of −400 mA·cm^{-2} (Fig. 5c).

To gain insight into the influence of the carbon layer on Cu@F-MC, the copper nanoparticle-loaded catalysts were prepared using a wet impregnation method based on the pre-synthesized F-MC network. TEM images show that catalysts prepared via the post-loaded method lack a carbon layer confined structure on the Cu sites, resulting in exposed Cu nanoparticles with a non-uniform size distribution ranging from 20 to 50 nm (Supplementary Figs. S6 and S7). Additionally, the zeta potentials of F-MC are measured before and after Cu loading. The results indicate that, unlike the Cu@F-MC structure obtained through co-assembly, the F-MC + Cu structure exhibits a positive zeta potential, which decreased following cationic functionalization (Fig. 5e). Due to the similarly charged interface between F-MC + Cu and cationic group, subsequent cationic groups modification is repelled, which limits the catalytic performance enhancement origining from the cationic effect.

The CO_2 electrocatalytic performance of F-MC + Cu was also evaluated. Specifically, compared to Cu@F-MC, the F-MC + Cu catalyst shows a preference for C_1 products and a limited suppression of HER, with FE of hydrogen exceeding 40% (Fig. 5f). In addition, FE_{C_2} product formation remains below 20% across a wide current widow. These findings confirm that the confinement effect of F-MC on copper sites is crucial for boosting the conversion of CO_2 into C_{2+} products. Moreover, a membrane electrode assembly (MEA) was constructed to evaluate the catalytic performance under industrial electrolysis. The MEA based on Cu@F-MC maintains high selectivity for C_{2+} products without significant degradation over 70 h continuous electrolysis. In contrast, F-MC + Cu demonstrates a rapid decline after just 15 h of reduction (Fig. 5g). This result indicates that the Cu@F-MC synthesized via the co-assembly method, with fluorinated mesoporous carbon layer, not only enhances the catalytic activity for CO_2RR toward valuable C_{2+} products, but also prevents the deactivation of active sites, thereby significantly extending the considerable stability.

3 Conclusions

In summary, we identified a fluorinated 2D mesoporous carbon confined copper catalyst for electrocatalytic CO_2RR. The unique confinement originated from 2D mesoporous carbon framework enabled the small size and homogeneous dispersion of Cu nanoparticles (~ 10 nm). This structure modulated local electronic structure of Cu nanoparticles, which drived the CO_2RR performance in promoting C_{2+} product formation. As a result, the Cu@F-MC catalyst generated C_{2+} products, primarily ethanol and acetic acid, and achieved a $FE_{C_{2+}}$ of 40.3%, primarily ethanol and acetic acid, under the current density of 400 mA·cm^{-2} and maintaining stability over 70h of continues electrolysis. Furthermore, the negatively charged interface provided by fluorine-functionalized carbon framework promoted cation anchoring via electrostatic interactions, further promoting C_2 selectivity. A $FE_{C_{2+}}$ of 63.9%, including ethanol conversion exceeding 40%, was attained in the cation-modulated Cu@F-MC. This strategy presents a promising approach to concurrently enhance the selectivity and stability of copper-based catalysts for the conversion of multi-carbon products.

References

[1] Arakawa, H.; Aresta, M.; Armor, J. N.; Barteau, M. A.; Beckman, E. J.; Bell, A. T.; Bercaw, J. E.; Creutz, C.; Dinjus, E.; Dixon, D. A. et al. Catalysis research of relevance to carbon management: Progress, challenges, and opportunities. *Chem. Rev.* **2001**, *101*, 953–996.

[2] Jouny, M.; Luc, W.; Jiao, F. General techno-economic analysis of CO_2 electrolysis systems. *Ind. Eng. Chem. Res.* **2018**, *57*, 2165–2177.

[3] Birdja, Y. Y.; Pérez-Gallent, E.; Figueiredo, M. C.; Göttle, A. J.; Calle-Vallejo, F.; Koper, M. T. M. Advances and challenges in understanding the electrocatalytic conversion of carbon dioxide to fuels. *Nat. Energy* **2019**, *4*, 732–745.

[4] Bushuyev, O. S.; De Luna, P.; Dinh, C. T.; Tao, L.; Saur, G.; van de Lagemaat, J.; Kelley, S. O.; Sargent, E. H. What should we make with CO_2 and how can we make it. *Joule* **2018**, *2*, 825–832.

[5] Yang, H. Y.; Zhang, C.; Gao, P.; Wang, H.; Li, X. P.; Zhong, L. S.; Wei, W.; Sun, Y. H. A review of the catalytic hydrogenation of carbon dioxide into value-added hydrocarbons. *Catal. Sci. Technol.* **2017**, *7*, 4580–4598.

[6] Guo, L. S.; Sun, J.; Ge, Q. J.; Tsubaki, N. Recent advances in direct catalytic hydrogenation of carbon dioxide to valuable C_{2+} hydrocarbons. *J. Mater. Chem. A* **2018**, *6*, 23244–23262.

[7] Ross, M. B.; De Luna, P.; Li, Y. F.; Dinh, C. T.; Kim, D.; Yang, P. D.; Sargent, E. H. Designing materials for electrochemical carbon dioxide recycling. *Nat. Catal.* **2019**, *2*, 648–658.

[8] Dokania, A.; Ramirez, A.; Bavykina, A.; Gascon, J. Heterogeneous catalysis for the valorization of CO_2: Role of bifunctional processes in the production of chemicals. *ACS Energy Lett.* **2019**, *4*, 167–176.

[9] Zhou, W.; Cheng, K.; Kang, J. C.; Zhou, C.; Subramanian, V.; Zhang, Q. H.; Wang, Y. New horizon in C_1 chemistry: Breaking the selectivity limitation in transformation of syngas and hydrogenation of CO_2 into hydrocarbon chemicals and fuels. *Chem. Soc. Rev.* **2019**, *48*, 3193–3228.

[10] Gao, D. F.; Arán-Ais, R. M.; Jeon, H. S.; Roldan Cuenya, B. Rational catalyst and electrolyte design for CO_2 electroreduction towards multicarbon products. *Nat. Catal.* **2019**, *2*, 198–210.

[11] Qiao, J. L.; Liu, Y. Y.; Hong, F.; Zhang, J. J. A review of catalysts for the electroreduction of carbon dioxide to produce low-carbon fuels. *Chem. Soc. Rev.* **2014**, *43*, 631–675.

[12] Nitopi, S.; Bertheussen, E.; Scott, S. B.; Liu, X. Y.; Engstfeld, A. K.; Horch, S.; Seger, B.; Stephens, I. E. L.; Chan, K.; Hahn, C. et al. Progress and perspectives of electrochemical CO_2 reduction on copper in aqueous electrolyte. *Chem. Rev.* **2019**, *119*, 7610–7672.

[13] Loiudice, A.; Lobaccaro, P.; Kamali, E. A.; Thao, T.; Huang, B. H.; Ager, J. W.; Buonsanti, R. Tailoring copper nanocrystals towards C_2 products in electrochemical CO_2 reduction. *Angew. Chem., Int. Ed.* **2016**, *55*, 5789–5792.

[14] De Luna, P.; Quintero-Bermudez, R.; Dinh, C. T.; Ross, M. B.; Bushuyev, O. S.; Todorović, P.; Regier, T.; Kelley, S. O.; Yang, P. D.; Sargent, E. H. Catalyst electro-redeposition controls morphology and oxidation state for selective carbon dioxide reduction. *Nat. Catal.* **2018**, *1*, 103–110.

[15] Jiang, K.; Sandberg, R. B.; Akey, A. J.; Liu, X. Y.; Bell, D. C.; Nørskov, J. K.; Chan, K.; Wang, H. T. Metal ion cycling of Cu foil for

selective C–C coupling in electrochemical CO_2 reduction. *Nat. Catal.* **2018**, *1*, 111–119.
[16] Li, J.; Xu, A. N.; Li, F. W.; Wang, Z. Y.; Zou, C. Q.; Gabardo, C. M.; Wang, Y. H.; Ozden, A.; Xu, Y.; Nam, D. H. et al. Enhanced multi-carbon alcohol electroproduction from CO via modulated hydrogen adsorption. *Nat. Commun.* **2020**, *11*, 3685.
[17] Li, Y. C.; Wang, Z. Y.; Yuan, T. G.; Nam, D. H.; Luo, M. C.; Wicks, J.; Chen, B.; Li, J.; Li, F. W.; de Arquer, F. P. G. et al. Binding site diversity promotes CO_2 electroreduction to ethanol. *J. Am. Chem. Soc.* **2019**, *141*, 8584–8591.
[18] Vasileff, A.; Xu, C. C.; Jiao, Y.; Zheng, Y.; Qiao, S. Z. Surface and interface engineering in copper-based bimetallic materials for selective CO_2 electroreduction. *Chem* **2018**, *4*, 1809–1831.
[19] Kim, T.; Palmore, G. T. R. A scalable method for preparing Cu electrocatalysts that convert CO_2 into C_{2+} products. *Nat. Commun.* **2020**, *11*, 3622.
[20] Zhang, J. W.; Zeng, G. M.; Zhu, S. Q.; Tao, H. L.; Pan, Y.; Lai, W. C.; Bao, J.; Lian, C.; Su, D.; Shao, M. H. et al. W. Steering CO_2 electroreduction pathway toward ethanol via surface-bounded hydroxyl species-induced noncovalent interaction. *Proc. Natl. Acad. Sci. USA* **2023**, *120*, e2218987120.
[21] Gu, J.; Liu, S.; Ni, W. Y.; Ren, W. H.; Haussener, S.; Hu, X. L. Modulating electric field distribution by alkali cations for CO_2 electroreduction in strongly acidic medium. *Nat. Catal.* **2022**, *5*, 268–276.
[22] Zhang, J.; My Pham, T. H.; Gao, Z. X.; Li, M.; Ko, Y.; Lombardo, L.; Zhao, W.; Luo, W.; Züttel, A. Electrochemical CO_2 reduction over copper phthalocyanine derived catalysts with enhanced selectivity for multicarbon products. *ACS Catal.* **2023**, *13*, 9326–9335.
[23] Wu, G. F.; Zhu, C.; Mao, J. N.; Li, G. H.; Li, S. J.; Dong, X.; Chen, A. H.; Song, Y. F.; Feng, G. H.; Liu, X. H. et al. Ampere-level CO_2-to-ethanol conversion via boron-incorporated copper electrodes. *ACS Energy Lett.* **2023**, *8*, 4867–4874.
[24] Popović, S.; Smiljanić, M.; Jovanovič, P.; Vavra, J.; Buonsanti, R.; Hodnik, N. Stability and degradation mechanisms of copper-based catalysts for electrochemical CO_2 reduction. *Angew. Chem., Int. Ed.* **2020**, *59*, 14736–14746.
[25] Kibria, G.; Dinh, C. T.; Seifitokaldani, A.; De Luna, P.; Burdyny, T.; Quintero-Bermudez, R.; Ross, M. B.; Bushuyev, O. S.; García de Arquer, F. P.; Yang, P. D. et al. A surface reconstruction route to high productivity and selectivity in CO_2 electroreduction toward C_{2+} hydrocarbons. *Adv. Mater.* **2018**, *30*, 1804867.
[26] Yu, L.; Deng, D. H.; Bao, X. H. Chain mail for catalysts. *Angew. Chem., Int. Ed.* **2020**, *59*, 15294–15297.
[27] Wan, Y. H.; Wang, C. Y.; Zhang, X. M.; Yin, Y.; Liu, M. M.; Ma, B.; Duan, L. L.; Ma, Y. Z.; Zhang, W.; Zheng, C. L. et al. Micelle-directed self-assembly of single-crystal-like mesoporous stoichiometric oxides for high-performance lithium storage. *Natl. Sci. Rev.* **2024**, *11*, nwae054.
[28] Sun, Z. K.; Sun, B.; Qiao, M. H.; Wei, J.; Yue, Q.; Wang, C.; Deng, Y. H.; Kaliaguine, S.; Zhao, D. Y. A general chelate-assisted co-assembly to metallic nanoparticles-incorporated ordered mesoporous carbon catalysts for Fischer–Tropsch synthesis. *J. Am. Chem. Soc.* **2012**, *134*, 17653–17660.
[29] Kim, J. Y.; Hong, D.; Lee, J. C.; Kim, H. G.; Lee, S.; Shin, S.; Kim, B.; Lee, H.; Kim, M.; Oh, J. et al. Quasi-graphitic carbon shell-induced Cu confinement promotes electrocatalytic CO_2 reduction toward C_{2+} products. *Nat. Commun.* **2021**, *12*, 3765.
[30] Zhang, W.; Zhang, J. W.; Wang, N.; Zhu, K. R.; Yang, C. C.; Ai, Y.; Wang, F. M.; Tian, Y.; Ma, Y. Z.; Ma, Y. et al. Two-electron redox chemistry via single-atom catalyst for reversible zinc-air batteries. *Nat. Sustain.* **2024**, *7*, 463–473.
[31] Zhang, W.; Zhu, K. R.; Yang, C. C.; Ai, Y.; Gao, Y. H.; Li, W.; Zhao, D. Y. Monomicelle-induced assembly route toward low-dimensional mesoporous nanomaterials for catalysis. *EcoEnergy* **2023**, *1*, 85–107.
[32] Wan, Y.; Qian, X. F.; Jia, N. Q.; Wang, Z. Y.; Li, H. X.; Zhao, D. Y. Direct triblock-copolymer-templating synthesis of highly ordered fluorinated mesoporous carbon. *Chem. Mater.* **2008**, *20*, 1012–1018.
[33] Chen, G.; Zhang, J. Y.; Yang, S. R. Fabrication of hydrophobic fluorinated amorphous carbon thin films by an electrochemical route. *Electrochem. Commun.* **2008**, *10*, 7–11.
[34] Dai, Y.; Cai, S. D.; Wu, L. J.; Yang, W. J.; Xie, J. Y.; Wen, W.; Zheng, J. C.; Zhu, Y. M. Surface modified CF_x cathode material for ultrafast discharge and high energy density. *J. Mater. Chem. A* **2014**, *2*, 20896–20901.
[35] Esmaeilirad, M.; Jiang, Z.; Harzandi, A. M.; Kondori, A.; Tamadoni Saray, M.; Segre, C. U.; Shahbazian-Yassar, R.; Rappe, A. M.; Asadi, M. Imidazolium-functionalized Mo_3P nanoparticles with an ionomer coating for electrocatalytic reduction of CO_2 to propane. *Nat. Energy* **2023**, *8*, 891–900.
[36] Qin, X. P.; Hansen, H. A.; Honkala, K.; Melander, M. M. Cation-induced changes in the inner- and outer-sphere mechanisms of electrocatalytic CO_2 reduction. *Nat. Commun.* **2023**, *14*, 7607.

Data availability

All data needed to support the conclusions in the paper are presented in the manuscript and the Supplementary Information. Additional data related to this paper may be requested from the corresponding author upon request.

Acknowledgements

This work was supported by the National Key Research and Development Program of China (No. 2022YFA1503501), the National Natural Science Foundation of China (Nos. 22088101 and U21A20329), Shanghai Pilot Program for Basic Research-FuDan University 21TQ1400100 (No. 21TQ008), Shanghai International Science and Technology Partnership Project (No. 23520750400), "Shuguang Program" supported by Shanghai Education Development Foundation and Shanghai Municipal Education Commission (No. 22SG02), and Fundamental Research Funds for the Central Universities (No. 20720220010).

Author contributions

Y. M., T. S. X., and W. L conceived the research and designed the experiments. Y. M. and T. S. X performed the experiment and analyzed the data. Y. M. wrote the manuscript. T. S. X., K. R. Z., and W. L. helped with characterization, revision, and polish of manuscript. W. L. and D. Y. Z. supervised the project.

Competing interests

The authors have no competing interests to declare that are relevant to this article.

Use of AI statement

None.

Additional information

Supplementary Information The online version contains supplementary material available at https://doi.org/10.26599/CF.2025.9200034.

Open Access This article is licensed under the terms of the Creative Commons Attribution 4.0 International License (http://creativecommons.org/licenses/by/4.0/), which permits use, sharing, distribution and reproduction in any medium, provided the original work is properly cited.

© The author(s) 2025. Published by Tsinghua University Press.